Composite Adaptive Super-Twisting Sliding Mode Control Using Barrier Function for PM Motor Drives Toward Electric Aircraft Applications

Qiankang Hou, Huanzhi Wang, *Graduate Student Member, IEEE*, Christopher H. T. Lee, *Senior Member, IEEE*, and Shihong Ding, *Senior Member, IEEE*

***Abstract*—To realize stable flight of electricaircraft in complex environments, this article investigates the composite adaptive super-twisting sliding mode (ASTSM) controller for permanent magnet (PM) motor drives utilized in aircraft electrical subsystems. In purpose of enhancing the flight control accuracy of electric aircraft, the large speed fluctuation and poor robustness existing in PM motor drive system have become the primary issues to be addressed. Distinct from the conventional super-twisting sliding mode controller that utilizes the conservative control gain to improve the performance of suppressing disturbance, the proposed barrier function based ASTSM control scheme can adjust the controller gain online according to the actual requirements. By utilizing the characteristics of the barrier function, the motor speed tracking error can be guaranteed to converge within a predefined region. In addition, the augmented input–output model based observer is adopted to compensate for the total disturbance, thereby enhancing the robustness of the electric aircraft flight control system. On this basis, the PM motor drive system can achieve satisfactory disturbance rejection ability without sacrificing its steady-state performance. Representative experimental results demonstrate the effectiveness of the proposed control approach.**

***Index Terms*—Adaptive super-twisting sliding mode (ASTSM), augmented input–output- model based observer, barrier function, electric aircraft, permanent magnet (PM) motor.**

I. Introduction

THE concept of electric aircraft has emerged as a pivotal trend in the future aviation industry, thanks to its promising features, such as low operating costs, superior reliability, and zero emissions. Through replacing hydraulic, pneumatic, and mechanical systems with electrical subsystems, the electric aircraft realize significant economic and environmental benefits [1], [2], [3], [4]. In recent years, permanent magnet (PM) motors have become an important part of the electric aircraft subsystems due to their simple structure and high efficiency [5]. Generally, the field-oriented control (FOC) scheme is utilized in PM motor drive systems to realize satisfactory tracking precision and response speed [6]. However, the time-varying disturbance caused by changing wind speed and air pressure negatively influence the stable operation and robustness of the PM motor. Consequently, effective suppression of the total disturbance is essential to achieve high-performance PM motor operation [7].

Although the traditional proportional-integral control approach has been maturely applied in FOC strategy, its performance is difficult to meet the requirements of high-efficiency operation of the PM motor under various complicated flight environments. In order to overcome the disadvantages of time-varying disturbance, active disturbance rejection control [8], fuzzy control [9], neural network control [10], sliding mode control (SMC) [11], [12], [13], and various modern control methods have been widely utilized to improve the disturbance rejection ability of PM motor drive systems. With the fast development of digital signal processors, the SMC is distinguished from the aforementioned modern algorithms due to its unique capabilities, such as strong robustness and low sensitivity to parameter uncertainty [14], [15], [16].

To achieve faster convergence speed and stronger disturbance suppression property, the terminal SMC scheme was developed in [17] to handle the drawbacks of conventional linear SMC. Nevertheless, the discontinuous switching terms existing in the first-order sliding mode controller can lead to chattering phenomenon, which affects the stable operation of the electric aircraft. Fortunately, the second-order sliding mode (SOSM) control strategy can perfectly solve the chattering problem without degrading the dynamic performance of the closed-loop system [18]. Without requiring the information about the derivative of the sliding variable, the super-twisting sliding mode (STSM) control algorithm has become the most widely used SOSM controller, and has been widely applied in PM motor drives [19], [20], [21].

Received 13 February 2025; revised 9 June 2025; accepted 3 July 2025. Date of publication 8 July 2025; date of current version 27 August 2025. This work was supported in part by the National Natural Science Foundation of China under Grant 62373170 and Grant 62403079, in part by the National Key Research and Development Program of China under Grant 2022YFD200150203, and in part by the Natural Science Foundation of Jiangsu Province under Grant BK20240963. Recommended for publication by Associate Editor O. Lucia. *(Corresponding authors: Christopher H. T. Lee; Shihong Ding.)*

Qiankang Hou is with the School of Mechanical Engineering and Rail Transit, Changzhou University, Changzhou 213164, China, also with the Jiangsu Key Laboratory of Green Process Equipment, Changzhou University, Changzhou 213164, China, and also with the School of Electrical and Information Engineering, Jiangsu University, Zhenjiang 212013, China (e-mail: hqk@cczu.edu.cn).

Huanzhi Wang and Christopher H. T. Lee are with the School of Electrical and Electronic Engineering, Nanyang Technological University, Singapore 639798 (e-mail: huanzhi001@e.ntu.edu.sg; chtlee@ntu.edu.sg).

Shihong Ding is with the School of Electrical and Information Engineering, Jiangsu University, Zhenjiang 212013, China (e-mail: dsh@ujs.edu.cn).

Color versions of one or more figures in this article are available at https://doi.org/10.1109/TPEL.2025.3587024.

Digital Object Identifier 10.1109/TPEL.2025.3587024

In order to produce a sufficiently large control effort to suppress the unknown disturbance, a conservative control gain needs to be selected, which may deteriorate the steady-state performance of the PM motor. To deal with the problem of excessive control gain, a gain-increasing adaptive super-twisting sliding mode (ASTSM) control scheme was employed in [22], which initially increases the control gain to ensure stable system operation, and then fixes the control gain at that value. Unfortunately, when the total disturbance decreases, this adaptive algorithm cannot reduce the control gain accordingly. In [23], an ASTSM control scheme based on the variation of control gain with disturbance amplitude was adopted for practical applications in the presence of time-varying disturbance. However, excessive parameters need to be adjusted in the aforementioned ASTSM controller, and the convergence range of the sliding mode variable relies on the upper boundary information of the unknown disturbance. Furthermore, some intelligent control methods have been adopted to regulate the gain of conventional STSM controller, such as fuzzy control and neural network control [24], [25]. However, the use of fuzzy rules and neural network technique requires powerful hardware computing performance and sufficient experimental data, which is difficult to achieve in the limited space and energy consumption of electric aircraft.

Aiming at further enhancing the antidisturbance capability and steady-state performance of PM motor drives utilized in electric aircraft, the disturbance compensation technique has drawn growing attention in recent years [26]. As is well known, the core of the disturbance compensation technique is the disturbance observer (DOB), which possesses the ability to estimate and compensate the total disturbance of the closed-loop system. In [27], the classical linear DOB put forward by Ohnishi was employed to estimate the unknown load torque and parameter uncertainties. However, as a highly complex nonlinear system, the PM motor drive system utilized in electric aircraft cannot be effectively linearized. To address this issue, the nonlinear DOB was constructed in [28], and the asymptotic convergence of the estimation error was proved by Lyapunov function. Combining the nonlinear DOB with the SMC algorithm, the tracking performance and robustness of the PM motor drive system can be significantly improved [29]. In [30], the novel DOB with augmented structure was utilized to estimate the total disturbance, which can obtain satisfactory disturbance and noise suppression performance. It should be noted that at least two tunable parameters are required to be adjusted in the above DOBs, which increases the parameter tunning workload in electric aircraft applications.

In light of the problem mentioned above, a barrier function based ASTSM control scheme combined with augmented input–output model based observer (AIOMBO) is proposed for PM motor drives toward electric aircraft applications. Experimental results show that the proposed control method can effectively improve the antidisturbance performance of the PM motor without sacrificing its steady-state performance. The main contribution of this article could be summarized in three aspects.

1) To avoid poor steady-state performance caused by overly conservative control gain, the barrier function is employed to adjust the control gain of STSM algorithm online. On this basis, the motor speed tracking error can be guaranteed to converge within the predefined region that meets practical requirements.
2) By adjusting the minimum value of the barrier function, the motor speed fluctuation caused by the periodic disturbance can be limited. Meanwhile, the speed drop generated by the aperiodic disturbance can be adjusted by tunning the boundary of the barrier function.
3) In view of the unfavorable effects of large current ripple and system noise, the novel and concise AIOMBO with augmented structure is adopted to compensate for the total disturbance. It should be noted that the performance of the AIOMBO can be changed by adjusting its unique parameter.

II. PM Motor Model Description and Conventional STSM Controller Design

A. Mathematical Model

In general, the speed equation of the PM motor drive system can be presented as

$$\dot{\Omega}_m = -\frac{B}{J}\Omega_m + \frac{T_e}{J} - \frac{T_L}{J} \tag{1}$$

where Ω_m is the motor speed, B is the frictional coefficient, J is the moment of inertia, T_e is the electromagnetic torque, and T_L denotes the load torque.

Taking the reference electromagnetic torque T_e^* as the control input, the motion equation can be reconstructed as

$$\dot{\Omega}_m = bT_e^* - bB\Omega_m - b\left(T_e^* - T_e\right) - bT_L \tag{2}$$

where $b = \frac{1}{J}$.

Considering the common inertia mismatch problem in PM motor drive system, the system model can be reconstructed into a general form

$$\begin{aligned}\dot{\Omega}_m &= b_0T_e^* + \left(b - b_0\right)T_e^* - bB\Omega_m \\ &\quad - b\left(T_e^* - T_e\right) - bT_L \\ &= b_0T_e^* - d_t\end{aligned} \tag{3}$$

where $d_t = -(b - b_0)T_e^* + bB\Omega_m + b(T_e^* - T_e) + bT_L$ is the total disturbance, $b_0 = \frac{1}{J_0}$, and J_0 denotes the nominal inertia.

B. Conventional STSM Controller Design

The conventional STSM control scheme is utilized as the speed controller for PM motor drive to suppress the total disturbance. By defining the reference motor speed signal as Ω_r, the speed tracking error Ω_e can be written as

$$\Omega_e = \Omega_m - \Omega_r. \tag{4}$$

Inspired by [11], the conventional STSM controller is given as

$$\begin{cases} T_e^* = -\alpha\lfloor\Omega_e\rceil^{1/2} + \upsilon \\ \dot{\upsilon} = -\beta \cdot \text{sign}\left(\Omega_e\right) \end{cases} \tag{5}$$

where α and β are adjustable controller parameters, and the notation $\lfloor\cdot\rfloor^n$ is defined as $\lfloor\cdot\rfloor^n = |\cdot|^n \cdot \text{sign}(\cdot)$ for a real number n. Specially, the values of parameters α and β can be selected as

$$\begin{cases} \alpha = 1.5\sqrt{D} \\ \beta = 1.1D \end{cases} \tag{6}$$

with D being the upper bound of $|\frac{\dot{d}_t}{b_0}|$.

Since the finite time stability of conventional STSM controller has been demonstrated by geometric approach and Lyapunov function [11], the stability analysis of STSM scheme is omitted here.

Remark 1: As shown in (6), parameter D determines the performance of the conventional STSM controller. Increasing the value of D can shorten the response time and improve the antidisturbance property of the PM motor drive system. However, larger parameter D may cause significant current ripple and excessive overshoot. In order to guarantee the stability of the PM motor drive system in the presence of time-varying disturbance, the information of the unknown upper bound D should be required [31], which is difficult to acquire during the operation of electric aircraft.

III. Proposed PM Motor Control Strategy

A. Barrier Function Based ASTSM Controller

In this section, the novel ASTSM controller is constructed to drive the PM motor system. Due to the characteristics of the barrier function, the proposed ASTSM controller can choose an appropriate controller gain without knowing the upper bound of the disturbance, thereby reducing the unwanted chattering phenomenon. The ASTSM algorithm is presented as follows:

$$\begin{cases} T_e^* = -h_1 L\left(\Omega_e(t)\right) \lfloor \Omega_e(t) \rfloor^{1/2} + \upsilon \\ \dot{\upsilon} = -h_2 L^2\left(\Omega_e(t)\right) \cdot \text{sign}\left(\Omega_e(t)\right) \end{cases} \tag{7}$$

where $h_1 = 1.5$ and $h_2 = 1.1$ are coefficients, and the adaptive law $L(\Omega_e(t))$ is designed as

$$L\left(\Omega_e(t)\right) = \begin{cases} L_1 t + L_2 & 0 \leqslant t \leqslant \bar{t} \\ L_b\left(\Omega_e(t)\right) & t > \bar{t} \end{cases} \tag{8}$$

with L_1 and L_2 being positive constants. Meanwhile, the form of barrier function $L_b(\Omega_e(t))$ is given as

$$L_b\left(\Omega_e(t)\right) = \frac{\varepsilon \bar{L}}{\varepsilon - |\Omega_e(t)|} \tag{9}$$

where $\bar{L}$ denotes the minimum value of the barrier function, and ε is related to the region of the barrier function. In addition, the schematic illustration of barrier function is shown in Fig. 1.

According to adaptive law (8), it is evident that the adaptive adjustment of the control gain of ASTSM scheme is divided into two steps. The first step is to employ the monotonically increasing adaptive law $L_1 t + L_2$ to increase the controller gain, so that the speed tracking error Ω_e can converge to region $[-\frac{\varepsilon}{2}, \frac{\varepsilon}{2}]$ at time $\bar{t}$. The second step is to adopt the barrier function to adjust the controller gain online to ensure that the speed tracking error stays within region $(-\varepsilon, \varepsilon)$. Specifically, when the motor speed tracking error gradually converges to the origin, the controller gain will be dynamically adjusted to a smaller value. On the contrary, when the tracking error gradually approaches the boundary of the predefined region, the controller gain can be dynamically tuned to a larger value to prevent the error from escaping out of the predefined region.

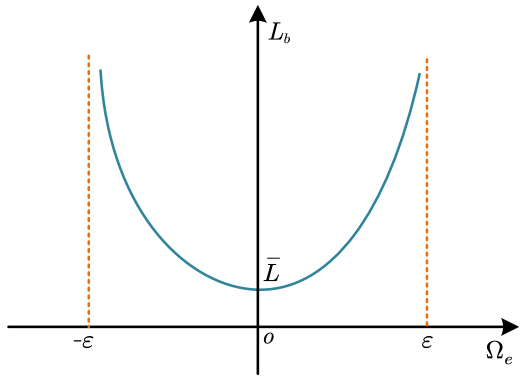

Fig. 1. Schematic illustration of barrier function L_b.

Remark 2: The parameter L_2 defines the initial value of the adaptive law, which needs to be chosen sufficiently large to ensure the stability of the PM motor drive system at the initial step. When the initial value of speed tracking error is far from the origin, a larger parameter L_2 can effectively improve the convergence rate of the tracking error. Similarly, increasing the value of parameter L_1 can enhance the convergence speed proportionally. When the speed tracking error is far from zero, a larger parameter L_1 is very useful for shortening the convergence time $\bar{t}$. However, excessively large parameters L_1 and L_2 may lead to overestimation of controller gain.

Remark 3: The parameter ε defines the upper bound of the speed tracking error. Obviously, decreasing the value of ε can increase the output signal of the barrier function, thereby improving the dynamic performance of the PM motor system. Unfortunately, significantly small parameter ε may cause the tough issues of output saturation and unwanted chattering phenomenon. The parameter $\bar{L}$ is related to the minimum value of the barrier function. Increasing the value of $\bar{L}$ can obviously optimize the disturbance rejection capacity of the PM motor drive system. Since the periodic disturbance always exists in the PM motor system, a larger parameter $\bar{L}$ can significantly reduce the speed fluctuation of the motor. However, an excessively large parameter $\bar{L}$ may cause the controller gain calculated by barrier function to be conservative.

Assumption 1: There exists a positive constant D^+ such that $|\dot{d}_t| \leq D^+$.

Remark 4: The derivative of the total disturbance d_t only needs to be bounded, and no prior knowledge of its exact upper bound is required, i.e., the constant D only needs to exist. Compared with other conventional adaptive algorithms, the above feature is the most significant advantage of the proposed ASTSM control method based on the barrier function.

Theorem 1: Under the ASTSM controller (7), the speed error of the PM drive system Ω_e will converge to the region $[-\frac{\varepsilon}{2}, \frac{\varepsilon}{2}]$ at some time $\bar{t}$ and remain in the region $(-\varepsilon, \varepsilon)$.

Proof: Since the adaptive law $L_1 t + L_2$ is monotonically increasing, the motor speed error will converge to the region $[-\frac{\varepsilon}{2}, \frac{\varepsilon}{2}]$ at some time $\bar{t}$. Then, we will demonstrate that the speed error will remain within the predefined region $(-\varepsilon, \varepsilon)$.

Regarding $s_1 = \Omega_e$ and $s_2 = b_0 v - d_t$, one has

$$\begin{cases} \dot{s}_1 = -b_0 h_1 L_b(s_1) \lfloor s_1 \rceil^{1/2} + s_2 \\ \dot{s}_2 = -b_0 h_2 L_b^2(s_1) \cdot \text{sign}(s_1) - \dot{d}_t. \end{cases} \tag{10}$$

Inspired by [32], constructing the following Lyapunov function:

$$V = b_0 h_2 \varepsilon \bar{L} L_b(s_1) + |s_1| + \frac{1}{2} s_2^2. \tag{11}$$

By a simple calculation, one has

$$\begin{aligned} \dot{V} &= \frac{b_0 h_2 \varepsilon^2 \bar{L}^2 \dot{s}_1 \cdot \text{sign}(s_1)}{(\varepsilon - |s_1|)^2} + \dot{s}_1 \cdot \text{sign}(s_1) + s_2 \dot{s}_2 \\ &= \frac{b_0 h_2 \varepsilon^2 \bar{L}^2 s_2 \cdot \text{sign}(s_1)}{(\varepsilon - |s_1|)^2} - \frac{b_0^2 h_2 \varepsilon^2 \bar{L}^2 h_1 L_b(s_1) |s_1|^{\frac{1}{2}}}{(\varepsilon - |s_1|)^2} \\ &\quad + s_2 \cdot \text{sign}(s_1) - b_0 h_1 L_b(s_1) |s_1|^{\frac{1}{2}} + s_2 \\ &\quad \times \left(-b_0 h_2 L_b^2(s_1) \cdot \text{sign}(s_1) - \dot{d}_t \right) \\ &= \frac{b_0 h_2 \varepsilon^2 \bar{L}^2 s_2 \cdot \text{sign}(s_1)}{(\varepsilon - |s_1|)^2} - \frac{b_0^2 h_2 \varepsilon^3 \bar{L}^3 h_1 |s_1|^{\frac{1}{2}}}{(\varepsilon - |s_1|)^3} \\ &\quad + s_2 \cdot \text{sign}(s_1) - \frac{b_0 h_1 \varepsilon \bar{L} |s_1|^{\frac{1}{2}}}{(\varepsilon - |s_1|)} \\ &\quad - \frac{s_2 b_0 h_2 \varepsilon^2 \bar{L}^2 \cdot \text{sign}(s_1)}{(\varepsilon - |s_1|)^2} - s_2 \dot{d}_t \\ &= -\frac{b_0^2 h_2 \varepsilon^3 \bar{L}^3 h_1 |s_1|^{\frac{1}{2}}}{(\varepsilon - |s_1|)^3} + s_2 \cdot \text{sign}(s_1) - \frac{b_0 h_1 \varepsilon \bar{L} |s_1|^{\frac{1}{2}}}{(\varepsilon - |s_1|)} \\ &\quad - s_2 \dot{d}_t \leqslant -\frac{b_0^2 h_2 \varepsilon^3 \bar{L}^3 h_1 |s_1|^{\frac{1}{2}}}{(\varepsilon - |s_1|)^3} \\ &\quad - \frac{b_0 h_1 \varepsilon \bar{L} |s_1|^{\frac{1}{2}}}{(\varepsilon - |s_1|)} + |s_2| - s_2 D^+. \end{aligned} \tag{12}$$

For the sake of simplicity, define $\Pi = |s_2| - s_2 D^+$. Thus, from (12), one obtains

$$\begin{aligned} \dot{V} &\leqslant -\frac{b_0^2 h_2 \varepsilon^3 \bar{L}^3 h_1 |s_1|^{\frac{1}{2}}}{(\varepsilon - |s_1|)^3} - \frac{b_0 h_1 \varepsilon \bar{L} |s_1|^{\frac{1}{2}}}{(\varepsilon - |s_1|)} + \Pi \\ &= -\frac{b_0^2 h_2 \varepsilon^3 \bar{L}^3 h_1 |s_1|^{\frac{1}{2}}}{(\varepsilon - |s_1|)^3} - \frac{1}{(\varepsilon - |s_1|)} \cdot \\ &\quad \left(b_0 h_1 \varepsilon \bar{L} |s_1|^{\frac{1}{2}} - \Pi \varepsilon + \Pi |s_1| \right) \\ &= -\frac{b_0^2 h_2 \varepsilon^3 \bar{L}^3 h_1 |s_1|^{\frac{1}{2}}}{(\varepsilon - |s_1|)^3} - \frac{\Pi}{(\varepsilon - |s_1|)} \cdot \\ &\quad \left(\frac{b_0 h_1 \varepsilon \bar{L} |s_1|^{\frac{1}{2}}}{\Pi} - \varepsilon + |s_1| \right) \\ &= -\frac{b_0^2 h_2 \varepsilon^3 \bar{L}^3 h_1 |s_1|^{\frac{1}{2}}}{(\varepsilon - |s_1|)^3} - \frac{\Pi}{(\varepsilon - |s_1|)} \Psi \end{aligned} \tag{13}$$

where $\Psi = \frac{b_0 h_1 \varepsilon \bar{L} |s_1|^{\frac{1}{2}}}{\Pi} - \varepsilon + |s_1|$

Consider $\Psi = 0$ as a quadratic equation, and its two roots defined by

$$\begin{cases} |s_{11}|^{\frac{1}{2}} = \dfrac{-\frac{b_0 h_1 \varepsilon \bar{L}}{\Pi} + \left(\left(\frac{b_0 h_1 \varepsilon \bar{L}}{\Pi} \right)^2 + 4\varepsilon \right)^{\frac{1}{2}}}{2} \\ |s_{12}|^{\frac{1}{2}} = \dfrac{-\frac{b_0 h_1 \varepsilon \bar{L}}{\Pi} - \left(\left(\frac{b_0 h_1 \varepsilon \bar{L}}{\Pi} \right)^2 + 4\varepsilon \right)^{\frac{1}{2}}}{2}. \end{cases} \tag{14}$$

Since $|s_{12}|^{\frac{1}{2}}$ is negative, only the first root is valid. Then, one has

$$s_{11} = \pm \left(\frac{-\frac{b_0 h_1 \varepsilon \bar{L}}{\Pi} + \left(\left(\frac{b_0 h_1 \varepsilon \bar{L}}{\Pi} \right)^2 + 4\varepsilon \right)^{\frac{1}{2}}}{2} \right)^2. \tag{15}$$

With the help of $(\frac{b_0 h_1 \varepsilon \bar{L}}{\Pi})^2 + (2\varepsilon^{\frac{1}{2}})^2 < (\frac{b_0 h_1 \varepsilon \bar{L}}{\Pi} + 2\varepsilon^{\frac{1}{2}})^2$, it follows that:

$$\begin{aligned} |s_{11}| &< \left(\frac{-\frac{b_0 h_1 \varepsilon \bar{L}}{\Pi} + \left(\left(\frac{b_0 h_1 \varepsilon \bar{L}}{\Pi} + 2\varepsilon^{\frac{1}{2}} \right)^2 \right)^{\frac{1}{2}}}{2} \right)^2 \\ &= \left(\frac{-\frac{b_0 h_1 \varepsilon \bar{L}}{\Pi} + \left(\frac{b_0 h_1 \varepsilon \bar{L}}{\Pi} + 2\varepsilon^{\frac{1}{2}} \right)}{2} \right)^2 \\ &= \varepsilon. \end{aligned} \tag{16}$$

Once $|s_1| > |s_{11}|$, the function Ψ is positive. At this point, the two terms $-\frac{b_0^2 h_2 \varepsilon^3 \bar{L}^3 h_1 |s_1|^{\frac{1}{2}}}{(\varepsilon - |s_1|)^3}$ and $-\frac{\Pi}{(\varepsilon - |s_1|)} \Psi$ in (13) are negative. Therefore, the system state s_1 will remain in $|s_1| \leqslant |s_{11}| < \varepsilon$, i.e., the motor speed tracking error Ω_e will remain in the region $(-\varepsilon, \varepsilon)$. ■

Remark 5: In [33], the minimum value of the barrier function is related to the parameter selection of the monotonically increasing adaptive law and the time when the sliding variable first converges to the region $[-\frac{\varepsilon}{2}, \frac{\varepsilon}{2}]$. If the sliding variable is far away from the region $[-\frac{\varepsilon}{2}, \frac{\varepsilon}{2}]$, the minimum value of the barrier function will be large, thus aggravating the chattering phenomenon. In [34], the minimum control gain calculated by the barrier function is zero. To reduce the motor speed fluctuation, it is inappropriate to select the minimum output value of the barrier function as zero.

Remark 6: During the parameter selection process for the barrier function (9), the parameter $\bar{L}$ can be adjusted first according to the steady-state operation requirements of the PM motor. On this basis, the value of parameter ε can be determined according to the aperiodic disturbance suppression performance requirements of the motor.

B. Design of AIOMBO

It is well known that the time-varying total disturbance caused by load torque and system uncertainties have adverse effects on motor operation. To overcome these problems, a concise and effective AIOMBO with certain noise suppression property is constructed in this subsection to compensate the total disturbance. First of all, define $\mathring{\Omega}_m$ as the augmented state of the actual motor speed Ω_m, and system (3) can be rewritten as

$$\begin{cases} \dot{\mathring{\Omega}}_m = \Omega_m \\ \dot{\Omega}_m = b_0 T_e^* - d_t. \end{cases} \tag{17}$$

On this basis, the auxiliary system of (17) is designed as

$$\begin{cases} \dot{\bar{\mathring{\Omega}}}_m = \bar{\Omega}_m \\ \dot{\bar{\Omega}}_m = b_0 \bar{T}_e^* \end{cases} \tag{18}$$

where $\bar{T}_e^*$ and $\bar{\mathring{\Omega}}_m$ are the input and output signals of the auxiliary system (18), respectively. In addition, the input signal is calculated by

$$\bar{T}_e^* = K\left(\mathring{\Omega}_m - \bar{\mathring{\Omega}}_m\right) \tag{19}$$

with $K > 0$ being the observer parameter.

Then, the estimation value of the total disturbance is given by

$$\hat{d}_t = b_0\left(T_e^* - \bar{T}_e^*\right). \tag{20}$$

Theorem 2: If the AIOMBO is constructed as (18)–(20) and the observer parameter K is large enough, the estimation value $\hat{d}_t$ will converge to the total disturbance d_t.

Proof: According to (17)–(19), one has

$$\ddot{\bar{T}}_e^* = K\left(\dot{\Omega}_m - b_0 \bar{T}_e^*\right). \tag{21}$$

Both sides of (21) divided by $K\ddot{\bar{T}}_e^*$ obtain

$$\frac{1}{K} = \frac{\dot{\Omega}_m - b_0 \bar{T}_e^*}{\ddot{\bar{T}}_e^*}. \tag{22}$$

When parameter K tends to infinity, one yields $\dot{\Omega}_m - b_0\bar{T}_e^* = 0$. With the help of (17), one has $b_0 T_e^* - d_t - b_0\bar{T}_e^* = 0$. Therefore, it can be concluded that the total disturbance d_t can be estimated by $\hat{d}_t = b_0(T_e^* - \bar{T}_e^*)$ accurately. ■

Finally, combining the ASTSM controller with the novel AIOMBO, the composite ASTSM+AIOMBO controller can be constructed as

$$\begin{cases} T_e^* = -h_1 L\left(\Omega_e(t)\right)\lfloor \Omega_e(t)\rfloor^{1/2} + \upsilon - \frac{\hat{d}_t}{b_0} \\ \dot{\upsilon} = -h_2 L^2\left(\Omega_e(t)\right)\cdot \operatorname{sign}\left(\Omega_e(t)\right). \end{cases} \tag{23}$$

The block diagram of the proposed ASTSM+AIOMBO control scheme is shown in Fig. 2.

Remark 7: Overall, the advantages of the proposed AIOMBO are twofold. On the one hand, most of existing high-order disturbance observers fail to possess the ability to adjust one parameter to change the estimation performance. It is worth noting that only parameter K needs to be adjusted in AIOMBO, which greatly reduces the parameter tuning workload. On the other hand, the AIOMBO is driven by the augmented state of the actual motor speed rather than the actual motor speed contaminated by system noise, thereby decreasing the adverse effects of system noise to a certain extent.

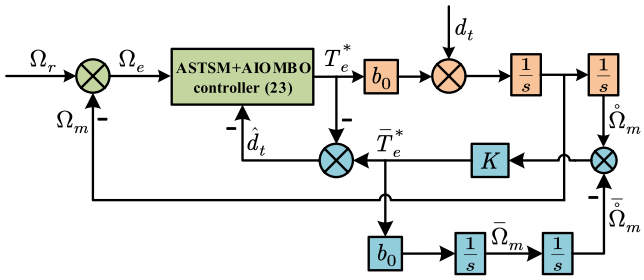

Fig. 2. Diagram of the proposed ASTSM+AIOMBO control scheme.

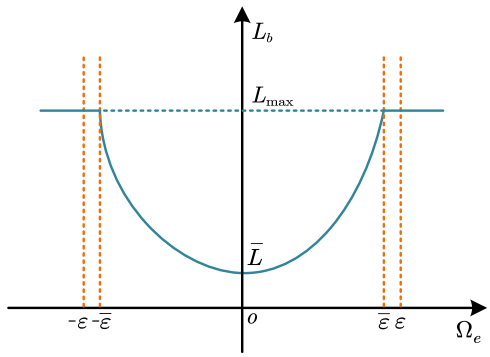

Fig. 3. Schematic illustration of barrier function with limited amplitude.

Remark 8: The parameter K determines the performance of the AIOMBO, which is crucial for the entire speed regulation system. A larger parameter K is desired for more precise estimation accuracy and stronger disturbance rejection capacity. However, increasing the value of parameter K will amplify the noise level in the closed-loop system. Therefore, K should be adjusted properly in compromise between the noise suppression performance and antidisturbance property.

Remark 9: If the electric aircraft encounters extreme working conditions or encoder failure during operation, causing the speed tracking error to escape the predefined region $(-\varepsilon, \varepsilon)$, the maximum output value of the barrier function can be predefined. The schematic illustration of the barrier function with limited amplitude is shown in Fig. 3. $L_{\max}$ is the maximum output of the barrier function that can generate the maximum control signal, that is, the maximum reference q-axis current. Parameter $\bar{\varepsilon}$ is selected to be close to the boundary ε. When the speed tracking error exceeds the boundary $(-\bar{\varepsilon}, \bar{\varepsilon})$, the output of the barrier function will become a fixed value $L_{\max}$, ensuring that the motor runs with the maximum reference q-axis current and quickly pulls the speed tracking error back to the region $(-\bar{\varepsilon}, \bar{\varepsilon})$. At this point, the difficulty in designing the control method for the PM motor drive system is transformed into the problem of designing the ASTSM controller under input saturation.

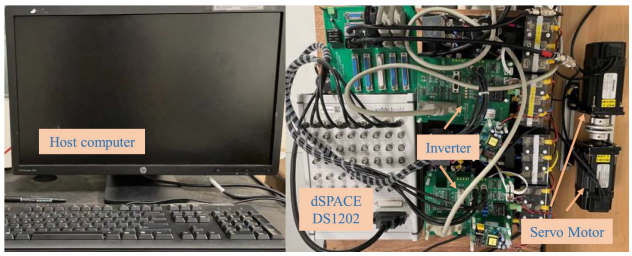

Fig. 4. Experimental setup of the PM motor drive system.

TABLE I
MOTOR AND SYSTEM PARAMETERS

Parameter	Symbol	Value and Unit
Stator inductance	L_s	5.7 mH
PM flux linkage	φ_f	0.092 wb
Rated power	P_N	0.75 kW
Moment of inertia	J	1.62×10^{-4} kg/m^2
Dc bus voltage	U_{dc}	150 V
Number of pole pairs	p_n	4
Stator resistance	R_s	1.1 Ω
Rated voltage	U_n	220 V
Rated torque	T_N	2.4 N · m

IV. EXPERIMENT RESULTS

In order to show the advantages of the proposed control strategy, several representative experiments are conducted in this section. Fig. 4 shows the test bench, and the rated parameters of the PM motor are summarized in Table I. The dSPACE DS1202 is employed to execute the control algorithms, and the classic FOC approach is utilized to drive the test PM motor. The sampling frequency is 10 kHz, and the reference q-axis current limit is 9 A. Meanwhile, the conventional input–output model based observer (IOMBO) is employed to compare with the proposed AIOMBO, and the IOMBO can be given as follows

$$\begin{cases} \hat{d}_t = b_0 \left(T_e^* - \bar{T}_e^*\right) \\ \bar{T}_e^* = K \left(\Omega_m - \bar{\Omega}_m\right) \\ \dot{\bar{\Omega}}_m = b_0 \bar{T}_e^* \end{cases} \tag{24}$$

where $\bar{T}_e^*$ and $\bar{\Omega}_m$ are the input and output signals of the auxiliary system $\dot{\bar{\Omega}}_m = b_0 \bar{T}_e^*$, respectively.

A. Comparative Experimental Results

Aiming at demonstrating the excellent properties of the proposed ASTSM+AIOMBO control method, the conventional STSM+IOMBO, ASTSM+IOMBO, and the proposed method are, respectively, conducted for the speed loop to compare their control performance. The value of parameter K in IOMBO and AIOMBO is chosen as $K = 400$. The control gain of ASTSM controller are calculated by the barrier function based adaptive law, and the parameters ε and $\bar{L}$ in adaptive law are selected as $\varepsilon = 3$ and $\bar{L} = 60$. The fixed parameter in conventional STSM controller is chosen as $\sqrt{D} = 160$. The results of the comparative experiment tests are given in Figs. 5 and 6.

Fig. 5 illustrates the experimental results of these three control strategies under load step, including motor speed, q-axis current, A-phase current, and control gain. Obviously, due to the ability to adjust the control gain in the presence of load step, the dynamic performance of the proposed ASTSM controller is better than conventional STSM control strategy. It can be observed from the results of q-axis current that the current ripple of ASTSM controller is smaller than STSM controller. However, since the control gain of conventional STSM controller is conservative, the speed fluctuation under STSM controller is smaller than that of ASTSM controller. In addition, compared with ASTSM+IOMBO control scheme, the proposed ASTSM+AIOMBO algorithm has better noise suppression property.

The experimental results of three different control schemes under sinusoidal reference are given in Fig. 6, including motor speed, speed error, A-phase current, and control gain. The sinusoidal reference speed signal is selected as $\Omega_m = 600\sin(\pi t)$. With the help of barrier function to automatically adjust the control gain, the maximum value of speed tracking error under ASTSM scheme is smaller than conventional STSM controller. In addition, the maximum value of speed tracking error under ASTSM+AIOMBO control strategy is similar to ASTSM+IOMBO algorithm. It should be noted that utilizing the AIOMBO with augmented structure can reduce the speed tracking error fluctuation. In summary, the proposed ASTSM+AIOMBO control approach outperforms other comparative control schemes and is more suitable for electric aircraft applications due to its satisfactory disturbance rejection ability.

B. Influence of Parameters in Barrier Function

To verify the influence of parameters in barrier function on the performance of the proposed ASTSM controller, comparative experimental results are presented in this subsection. Figs. 7 and 8 illustrate the results of the proposed ASTSM+AIOMBO control strategy under different values of parameter ε, including the results of load variation and sinusoidal reference tracking. The specific choices for parameter ε are 2.5, 3.5, and 4.5, respectively. According to the theoretical analysis in the previous section, parameter ε determines the range of speed tracking error, which affects the disturbance rejection property of PM motor drive system. From the results of motor speed in Fig. 7, it can be seen that reducing parameter ε can significantly improve the dynamic performance of PM motor system, thereby decreasing the speed drop of the motor under load step. However, compared to the dynamic performance of the motor, the change in parameter ε seems to have limited impact on steady-state speed fluctuation. Similarly, it can be concluded in Fig. 8 that reducing parameter ε can obviously reduce the maximum value of motor speed tracking error, but has little impact on speed tracking error fluctuation.

The experimental results of the proposed control strategy under different values of parameter $\bar{L}$ are given in Figs. 9 and 10. The specific choices for parameter $\bar{L}$ are 80, 160, and 240, respectively. According to the theoretical analysis in the previous section, parameter $\bar{L}$ defines the minimum value of the barrier function, which influences the minimum values of parameters

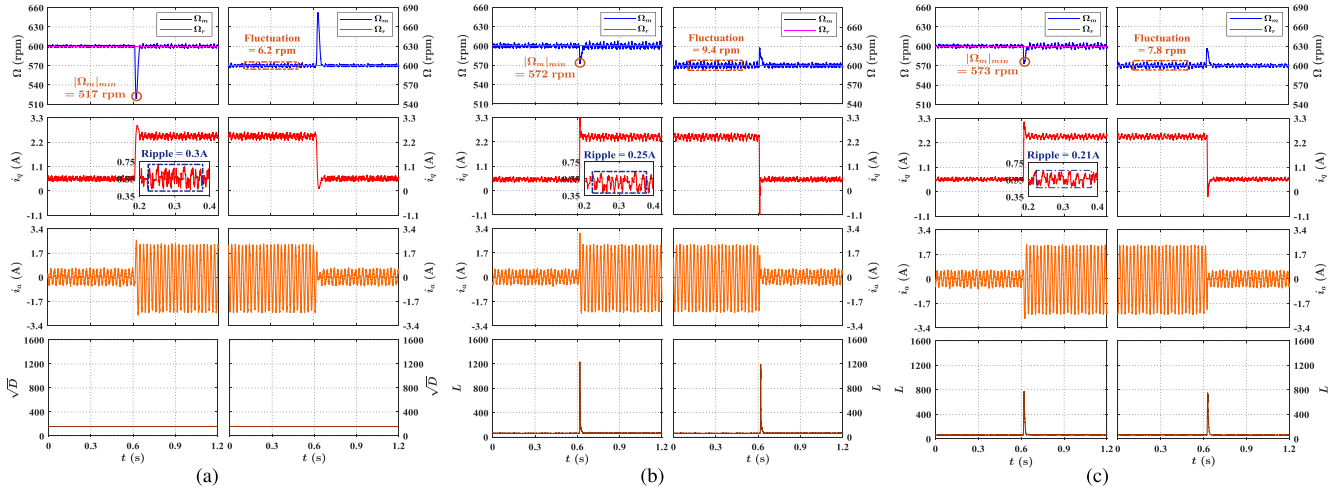

Fig. 5. Experimental results of three different control schemes under load step. (a) STSM+IOMBO. (b) ASTSM+IOMBO. (c) ASTSM+AIOMBO.

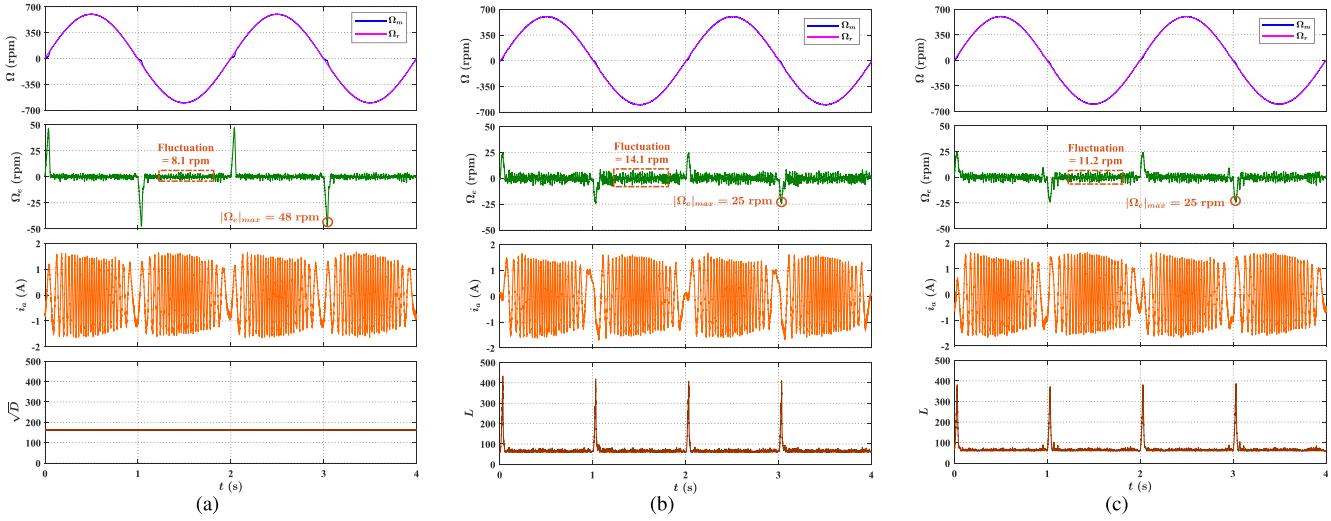

Fig. 6. Experimental results of three different control schemes under sinusoidal reference. (a) STSM+IOMBO. (b) ASTSM+IOMBO. (c) ASTSM+AIOMBO.

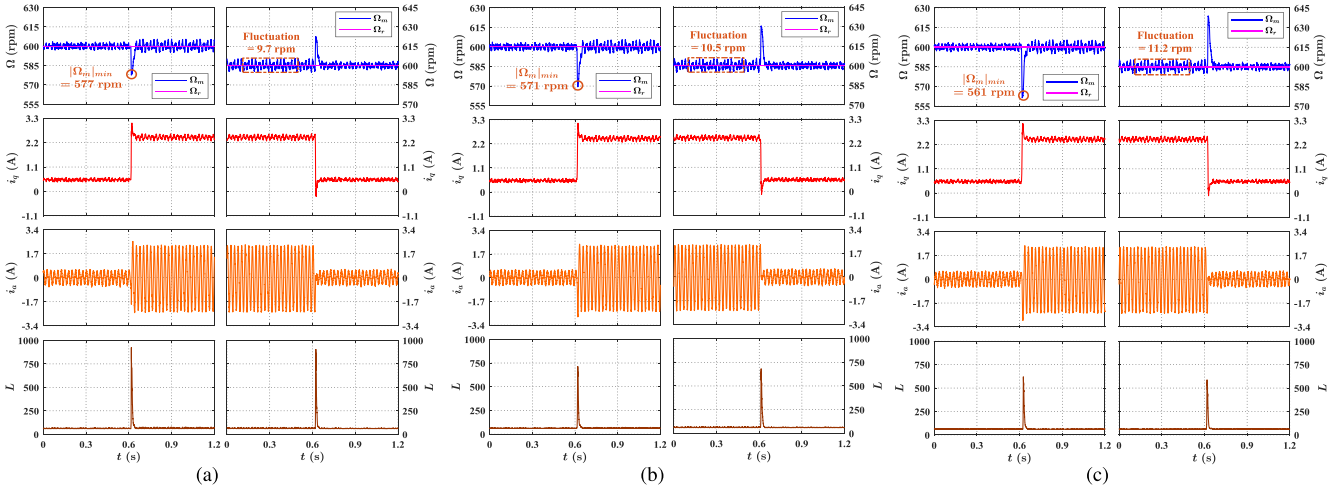

Fig. 7. Experimental results of different parameter ε under load step. (a) $\varepsilon = 2.5$. (b) $\varepsilon = 3.5$. (c) $\varepsilon = 4.5$.

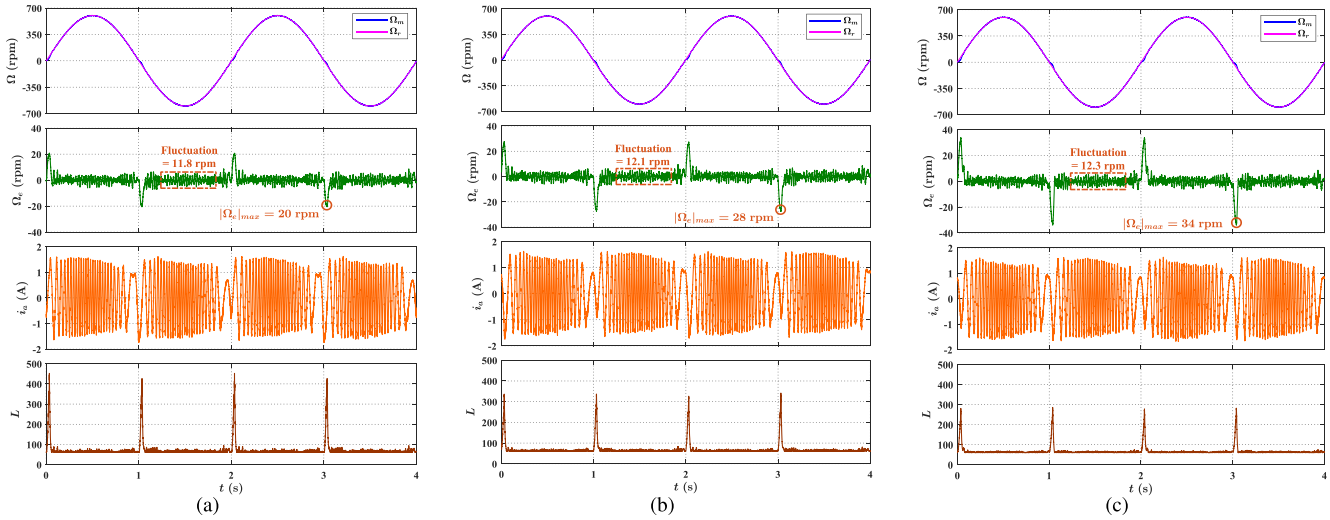

Fig. 8. Experimental results of different parameter ε under sinusoidal reference. (a) $\varepsilon = 2.5$. (b) $\varepsilon = 3.5$. (c) $\varepsilon = 4.5$.

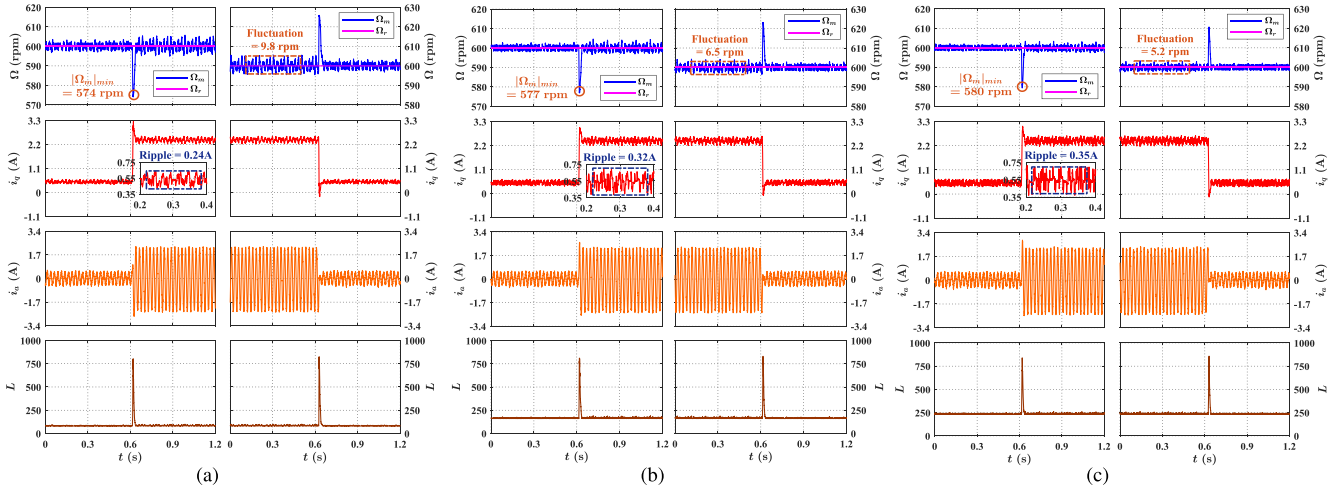

Fig. 9. Experimental results of different parameter $\bar{L}$ under load step. (a) $\bar{L} = 80$. (b) $\bar{L} = 160$. (c) $\bar{L} = 240$.

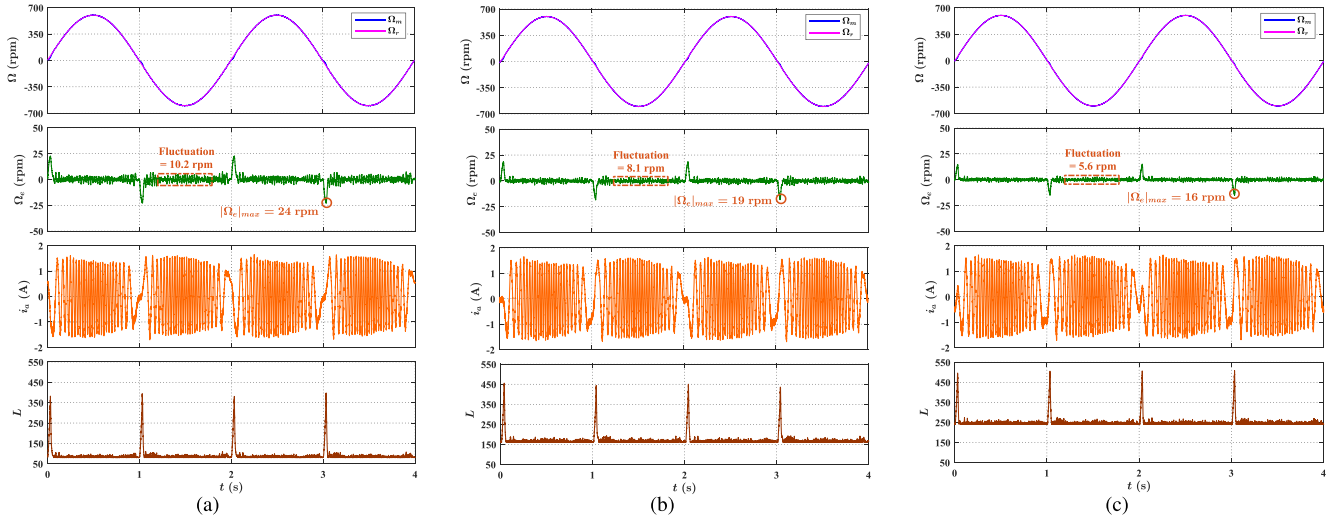

Fig. 10. Experimental results of different parameter $\bar{L}$ under sinusoidal reference. (a) $\bar{L} = 80$. (b) $\bar{L} = 160$. (c) $\bar{L} = 240$.

in the proposed ASTSM controller. Obviously, increasing the value of parameter $\bar{L}$ can significantly reduce the steady-state speed fluctuation, which means that the periodic disturbance rejection property of PM motor system is improved. However, increasing parameter $\bar{L}$ will result in larger current ripple, which may affect the long-term operation of the motor. Meanwhile, according to the tracking results in Fig. 10, increasing parameter $\bar{L}$ can obviously reduce the maximum value of the motor speed tracking error fluctuation.

V. Conclusion

In this article, a combination of the ASTSM controller and AIOMBO algorithm is constructed for PM motor drive systems toward electric aircraft applications. Compared with the conventional STSM controller with fixed and conservative control gain, the barrier function is adopted to adjust the control gain of STSM algorithm online without requiring the knowledge of the total disturbance. On this basis, the dynamic performance of PM motor system can be significantly enhanced. Meanwhile, the novel AIOMBO with only one parameter is employed to compensate the total disturbance, thereby reducing the adverse effects of large current ripple. Finally, rigorous theoretical analysis and comprehensive experiments demonstrate the validity of the proposed control strategy. Our future research will be focused on extending the proposed method to applications with low sampling frequencies and input saturation scenarios.

References

[1] Z. R. Zhang, Y. Liu, and J. C. Li, "A HESM-based variable frequency AC starter-generator system for aircraft applications," *IEEE Trans. Energy Convers.*, vol. 33, no. 4, pp. 1998–2006, Dec. 2018.

[2] B. Sarlioglu and C. T. Morris, "More electric aircraft: Review, challenges, and opportunities for commercial transport aircraft," *IEEE Trans. Transport. Electrific.*, vol. 1, no. 1, pp. 54–64, Jun. 2015.

[3] J. W. Lu, Z. R. Zhang, J. C. Li, and H. Shi, "A single-stage control strategy of wound-rotor synchronous starter generator under excitation failure conditions for hybrid-electric propulsion aircraft application," *IEEE Trans. Transport. Electrific.*, vol. 10, no. 3, pp. 5368–5378, Sep. 2024.

[4] J. L. Sun, S. C. Xu, S. H. Ding, Z. Q. Pu, and J. Q. Yi, "Adaptive conditional disturbance negation-based nonsmooth-integral control for PMSM drive system," *IEEE-ASME Trans. Mechatron.*, vol. 29, no. 5, pp. 3602–3613, Oct. 2024.

[5] Y. Z. Chen, T. Yang, L. H. Fan, and S. Bozhko, "Sensorless control design of high-speed electric drives in discrete-time domain for mild-hybrid turboprop aircraft applications," *IEEE Trans. Transport. Electrific.*, vol. 9, no. 3, pp. 3601–3619, Sep. 2023.

[6] Q. K. Hou, S. H. Ding, X. H. Yu, and K. Q. Mei, "A super-twisting-like fractional controller for SPMSM drive system," *IEEE Trans. Ind. Electron.*, vol. 69, no. 9, pp. 9376–9384, Sep. 2022.

[7] F. X. Wang, Y. Wei, H. Young, D. L. Ke, H. T. Xie, and J. Rodriguez, "Continuous-control-set model-free predictive fundamental current control for PMSM system," *IEEE Trans. Power Electron.*, vol. 38, no. 5, pp. 5928–5938, May 2023.

[8] Y. F. Zuo, X. Y. Zhu, L. Quan, C. Zhang, Y. Du, and Z. X. Xiang, "Active disturbance rejection controller for speed control of electrical drives using phase-locking loop observer," *IEEE Trans. Ind. Electron.*, vol. 66, no. 3, pp. 1748–1759, Mar. 2019.

[9] L. Shanmugam and Y. H. Joo, "Design of interval type-2 fuzzy-based sampled-data controller for nonlinear systems using novel fuzzy Lyapunov functional and its application to PMSM," *IEEE Trans. Syst., Man, Cybern., Syst.*, vol. 51, no. 1, pp. 542–551, Jan. 2021.

[10] C. L. Xia, C. Guo, and T. N. Shi, "A neural-network-identifier and fuzzy-controller-based algorithm for dynamic decoupling control of permanent-magnet spherical motor," *IEEE Trans. Ind. Electron.*, vol. 57, no. 8, pp. 2868–2878, Aug. 2010.

[11] Q. K. Hou, S. H. Ding, and X. H. Yu, "Composite super-twisting sliding mode control design for PMSM speed regulation problem based on a novel disturbance observer," *IEEE Trans. Energy Convers.*, vol. 36, no. 4, pp. 2591–2599, Dec. 2021.

[12] L. Zhang, Z. Y. Chen, X. H. Yu, J. Yang, and S. H. Li, "Sliding-mode-based robust output regulation and its application in PMSM servo systems," *IEEE Trans. Ind. Electron.*, vol. 70, no. 2, pp. 1852–1860, Feb. 2023.

[13] K. Yu, S. H. Li, W. W. Zhu, and Z. Wang, "Sensorless control scheme for PMSM drive via generalized proportional integral observers and Kalman filter," *IEEE Trans. Power Electron.*, vol. 40, no. 3, pp. 4020–4033, Mar. 2025.

[14] J. Q. Yang, C. X. Yang, X. F. Zhang, and J. Na, "Fixed-time sliding mode control with varying exponent coefficient for modular reconfigurable flight arrays," *IEEE/CAA J. Autom. Sinica*, vol. 11, no. 2, pp. 514–528, Feb. 2024.

[15] J. L. Sun, J. Xia, S. H. Ding, and X. H. Yu, "Exact-feedback-linearization-based adaptive second-order sliding mode control design for DC-DC boost converters," *IEEE Trans. Ind. Electron.*, vol. 72, no. 5, pp. 5397–5407, May 2025.

[16] Q. K. Hou et al., "Super-twisting extended state observer-based quasi-proportional-resonant controller for permanent magnet synchronous motor drive system," *IEEE Trans. Transport. Electrific.*, vol. 10, no. 1, pp. 1596–1604, Mar. 2024.

[17] S. H. Yu, X. H. Yu, B. Shirinzadeh, and Z. H. Man, "Continuous finite-time control for robotic manipulators with terminal sliding mode," *Automatica*, vol. 41, no. 11, pp. 1957–1964, Nov. 2005.

[18] J. Song, W. X. Zheng, and Y. G. Niu, "Self-triggered sliding mode control for networked PMSM speed regulation system: A PSO-optimized super-twisting algorithm," *IEEE Trans. Ind. Electron.*, vol. 69, no. 1, pp. 763–773, Jan. 2022.

[19] D. X. Fu, X. M. Zhao, and J. G. Zhu, "A novel robust super-twisting nonsingular terminal sliding mode controller for permanent magnet linear synchronous motors," *IEEE Trans. Power Electron.*, vol. 37, no. 3, pp. 2936–2945, Mar. 2022.

[20] A. Nurettin and N. Inanc, "High-performance induction motor speed control using a robust hybrid controller with a supertwisting sliding mode load disturbance observer," *IEEE Trans. Ind. Electron.*, vol. 70, no. 8, pp. 7743–7752, Aug. 2023.

[21] L. Chen, H. M. Zhang, H. Wang, K. Shao, G. Y. Wang, and A. Yazdani, "Continuous adaptive fast terminal sliding mode-based speed regulation control of PMSM drive via improved super-twisting observer," *IEEE Trans. Ind. Electron.*, vol. 71, no. 5, pp. 5105–5115, May 2024.

[22] G. P. Incremona, M. Cucuzzella, and A. Ferrara, "Adaptive suboptimal second-order sliding mode control for microgrids," *Int. J. Control*, vol. 89, no. 9, pp. 1849–1867, 2016.

[23] D. Y. Negrete-Chavez and J. A. Moreno, "Second-order sliding mode output feedback controller with adaptation," *Int. J. Adapt. Control Signal Process.*, vol. 30, no. 8–10, 1523-1543, Aug. 2016.

[24] F. Zhang and P. F. Huang, "Fuzzy-based adaptive super-twisting sliding-mode control for a maneuverable tethered space net robot," *IEEE Trans. Fuzzy Syst.*, vol. 29, no. 7, pp. 1739–1749, Jul. 2021.

[25] F. F. M. El-Sousy, M. M. Amin, and O. A. Mohammed, "Robust adaptive neural network tracking control with optimized super-twisting sliding-mode technique for induction motor drive system," *IEEE Trans. Ind. Appl.*, vol. 58, no. 3, pp. 4134–4157, May/Jun. 2022.

[26] H. Y. Cao, Y. T. Deng, J. Liu, Y. Zuo, X. F. Liu, and H. Z. Wang, "Improved deadbeat predictive current control of PMSM drives with repetitive control-based disturbance correction observer," *IEEE Trans. Power Electron.*, vol. 40, no. 1, pp. 801–812, Jan. 2025.

[27] S. K. Kim and K. B. Lee, "Surface stabilizing speed-tracking control for PMSMs via loop adaptation and order reduction approaches," *IEEE J. Emerg. Sel. Topics Power Electron.*, vol. 11, no. 1, pp. 545–555, Feb. 2023.

[28] W. H. Chen, D. J. Ballance, P. J. Gawthrop, and J. O'Reilly, "A nonlinear disturbance observer for robotic manipulators," *IEEE Trans. Ind. Electron.*, vol. 47, no. 4, pp. 932–938, Aug. 2000.

[29] A. Apte, U. Thakar, and V. Joshi, "Disturbance observer based speed control of PMSM using fractional order PI controller," *IEEE/CAA J. Autom. Sin.*, vol. 6, no. 1, pp. 316–326, Jan. 2019.

[30] Q. K. Hou et al., "Enhanced active disturbance rejection control with measurement noise suppression for PMSM drives via augmented nonlinear extended state observer," *IEEE Trans. Energy Convers.*, vol. 39, no. 1, pp. 287–299, Mar. 2024.
[31] M. J. Hu, W. Hua, Z. Wang, S. H. Li, P. X. Wang, and Y. C. Wang, "Selective periodic disturbance elimination using extended harmonic state observer for smooth speed control in PMSM drives," *IEEE Trans. Power Electron.*, vol. 37, no. 11, pp. 13288–13298, Nov. 2022.
[32] H. Obeid, L. Fridman, S. Laghrouche, M. Harmouche, and M. A. Golkani, "Adaptation of levant's differentiator based on barrier function," *Int. J. Control*, vol. 91, no. 9, pp. 2019–2027, 2018.
[33] H. Obeid, S. Laghrouche, L. Fridman, Y. Chitour, and M. Harmouche, "Barrier function-based adaptive super-twisting controller," *IEEE Trans. Autom. Control*, vol. 65, no. 11, pp. 4928–4933, Nov. 2020.
[34] K. Shao, J. C. Zheng, H. Wang, X. Q. Wang, R. Q. Lu, and Z. H. Man, "Tracking control of a linear motor positioner based on barrier function adaptive sliding mode," *IEEE Trans. Ind. Inf.*, vol. 17, no. 11, pp. 7479–7488, Nov. 2021.

Qiankang Hou received the B.Eng. degree in electrical engineering and the Ph.D. degree in control science and engineering from Jiangsu University, Zhenjiang, China, in 2017 and 2023, respectively.

Since 2023, he has been with Changzhou University, Changzhou, China, where he is currently a Lecturer with the School of Mechanical Engineering. From December 2021 to December 2022, he visited the School of Electrical and Electronic Engineering, Nanyang Technological University, Singapore. His research interests include power electronics, electric machines and drives, and advanced control strategies.

Huanzhi Wang (Graduate Student Member, IEEE) received the B.Eng. degree in electrical engineering and automation from Dalian Maritime University, Dalian, China, in 2020, and the M.Sc. degree in power engineering in 2021 from Nanyang Technological University, Singapore, where he is currently working toward the Ph.D. degree in electrical and electronic engineering with the School of Electrical and Electronic Engineering.

His research interests include power electronics, electric motor drives, and advanced control strategies.

Christopher H. T. Lee (Senior Member, IEEE) received the B.Eng. (First Class Honours) degree in 2009, and Ph.D. degree in 2016, from Department of Electrical and Electronic Engineering, The University of Hong Kong, Hong Kong, both in electrical engineering.

He is currently an Associate Professor with Nanyang Technological University, Singapore. He was a Postdoctoral Fellow and then a Visiting Assistant Professor with the Massachusetts Institute of Technology, Cambridge, MA, USA. He has authored or coauthored two books, four books chapters, and more than 230 referred papers in the areas of his interest. His research interests include electric machines and drives, renewable energies, and electromechanical propulsion technologies.

Dr. Lee was a recipient of the 10th Nagamori Award in 2024, IAS Myron Zucker Student-Faculty Grant in 2023, JSPS Fellowship in 2023, MDPI Energies Young Investigator Award in 2022, NRF Fellowship in 2020, Nanyang Assistant Professorship in 2019, Li Ka Shing Prize (the best Ph.D. thesis prize) in 2017 and Croucher Foundation Fellowship in 2016, and five Best Paper Awards, including First Place Best Paper Award in IEEE Transactions on Energy Conversion in 2022. He is the Chair of IEEE Vehicular Technology Society Singapore Section Chapter in 2023–2025. He is a Chartered Engineer in Hong Kong. He is an Associate Editor for IEEE TRANSACTIONS ON INDUSTRIAL ELECTRONICS, IEEE TRANSACTIONS ON ENERGY CONVERSION, *IEEE Access, and IET Renewable Power Generation*.

Shihong Ding (Senior Member, IEEE) was born in Anhui, China, in 1983. He received the B.E. degree in mathematics from Anhui Normal University, China, in 2004, and the M.S. and Ph.D. degrees in automatic control from Southeast University, China, in 2007 and 2010, respectively.

Since 2010, he has been with the School of Electrical and Information Engineering, Jiangsu University, Zhenjiang, China, where he is currently a Full Professor. From 2008 to 2009, he visited The University of Texas at San Antonio, TX, USA. After graduation, he held a research fellowship with the University of Western Sydney, Penrith, Australia, for one year. In 2018, he visited Yeungnam University, South Korea, and from 2019 to 2020, with RMIT University, Melbourne, Australia. His research interests include sliding mode control and finite-time stability.

Dr. Ding also serves as a Subject Editor/Associate Editor for IEEE TRANSACTIONS ON INDUSTRIAL ELECTRONICS, *Nonlinear Dynamics*, and *International Journal of Adaptive Control and Signal Processing*.